Available online at
https://journal.uitm.edu.my/ojs/index.php/MJCET

e-ISSN: 2682-8588

Malaysian Journal of Chemical Engineering & Technology 8(2) 2025, 126–145

Malaysian Journal of Chemical Engineering and Technology

Effect of drying temperature on synthesised zinc oxide microparticles from mango seed extract

Nurainul Kamalia Iskandar Hussein[1], Rabiatul Adawiyah Abdol Aziz[2*], Siti Fatma Abd Karim[3], Ummi Kalthum Ibrahim[4]

[1,2,3,4]*Faculty of Chemical Engineering, Universiti Teknologi MARA,40450 Shah Alam, Selangor, Malaysia*

ARTICLE INFO

Article history:
Received 31 July Month 2025
Revised 27 October 2025
Accepted 29 October 2025
Online first
Published 31 October 2025

Keywords:
Capping agent
Biological synthesis
Mangifera indica seed
Green chemistry
Sustainable material

DOI:
10.24191/mjcet.v8i2.8252

ABSTRACT

Zinc oxide (ZnO) is known for its antimicrobial activity, UV protection, and applications in environmental fields. However, the green synthesis of ZnO is often affected by processing conditions, especially drying temperature. This study investigates the effect of drying temperatures at 60, 70, and 80 °C on ZnO synthesis using mango seed extract (MSE) as a natural reducing agent. Zinc acetate dihydrate (ZA) and zinc nitrate hexahydrate (ZN) were used as precursors to supply Zn^{2+} ions during synthesis. ZA samples produced higher extraction yields, with a maximum of 37.80% at 60 °C. All ZN samples powders appeared finer and brighter in colour. SEM images showed that ZA samples formed larger rod-like agglomerates, while ZN samples produced more uniform and less clustered particles with spherical or flower-like shapes. EDX confirmed the presence of only zinc and oxygen, with ZN samples showing more consistent Zn to O ratios across all temperatures. Zeta potential analysis indicated that ZN samples had more stable negative surface charges ranging from −22 to −25 mV. In contrast, ZA sample showed fluctuating values with a strong positive charge at 80 °C. Particle size analysis showed that ZN sample at 70 °C had the smallest and most uniform size of 1.454 µm, while ZA sample at 70 °C showed the largest particles. XRD confirmed that all samples followed the wurtzite crystal structure. Crystallite size increased with temperature in ZA samples but decreased slightly in ZN samples. FTIR analysis confirmed Zn–O stretching and showed fewer organic residues in ZN samples. UV-Vis results indicated that ZA had consistent absorption peaks and band gap values between 4.53 and 4.61 eV. ZN showed a strong band gap of 4.54 eV at 60 °C but dropped significantly at higher temperatures. Overall, ZN at 70 °C produced ZnO with the best morphology and surface stability, while ZA at 70 °C showed better optical performance and consistent band gap behaviour.

[2*]Corresponding author. *E-mail address*: rabia1338@uitm.edu.my

https://doi.org/10.24191/mjcet.v8i2.8252

1. INTRODUCTION

The unique features of zinc oxide (ZnO) particles, such as high stability, effective ultraviolet blocking (Irede et al., 2024), and broad-spectrum antimicrobial activity (Bekele et al., 2021; Thirumal et al., 2014; Yudaev et al., 2022), have made them widely explored in diverse fields, like pharmaceuticals, cosmetics, electronics, environmental remediation, and packaging applications (Al-darwesh et al., 2024). The conventional synthesis methods used for the preparation of ZnO are usually chemical or physical methods and they have a few drawbacks due to these methods are mostly performed using hazardous chemicals and high energy input, which raises environmental and safety concerns (Ahmed et al., 2017; Basnet et al., 2018). To addresses these issues, green synthesis using plant extracts has become popular eco-friendly and sustainable alternative methods of ZnO preparation (Shafey, 2020).

The plant-based green synthesis of ZnO particles uses natural chemicals in plants, known as phytochemicals, to reduce and stabilise zinc ions (Zn^{2+}) during synthesis process. These phytochemicals include flavonoids, phenolic compounds, terpenoids, and alkaloids, which have functional groups like hydroxyl (–OH), carboxyl (–COOH), and amine ($–NH_2$) to convert Zn^{2+} into ZnO and prevent the particles from agglomerate (Ahmed et al., 2017). Study by (Abdullahi Ari et al., 2023) shows the phenolic compounds in *Mangifera indica* can reduce Zn^{2+} and (Bishop et al., 2009) also reported that phenolic compounds can stabilise the particles using hydrogen bonds and van der Waals forces. Flavonoids such as quercetin and rutin, found in *Camellia sinensis* (Thirumal et al., 2014) and *Azadirachta indica* (Bhuyan et al., 2015), are powerful reducing agents due to their aromatic and conjugated structures. Terpenoids in *Aloe barbadensis* (aloe vera) act as both reducing and stabilizing agents, ensuring the particles are evenly formed (Ali et al., 2016). Alkaloids from *Catharanthus roseus* (periwinkle) provide stability by forming ionic and hydrogen bonds with their amine groups (Malaiappan et al., 2024).

Among all of the plants used for the synthesis, mango seeds (*Mangifera indica*) are a great option because they contain many helpful natural stabilizing compounds (Rajeshkumar et al., 2023). Flavonoids like quercetin, kaempferol, isoquercitrin and anthocyanins in mango seeds are strong reducing agents that can stop the particles from agglomerate. Phenolic compounds such as mangiferin and gallic acid in the seed also play an important role at keep the particles stable by forming protective layers around them. Mango seeds also have high contents of tannins (up to 20.7%) that enables the mango seed extract to bind with zinc ions effectively (Torres-León et al., 2016), helping to control the formation of ZnO particles into uniform sizes and shapes while providing protection from damage (Rajeshkumar et al., 2023). The combination of these natural compounds makes mango seeds very effective and reliable for ZnO synthesis. Using mango seeds, which are often thrown away, fits well with sustainable practices as they are not only cheap and easy to get but also environmentally friendly.

The most common zinc precursors used for synthesizing ZnO are zinc acetate (ZA) and zinc nitrate (ZN), each with unique benefits. ZA is a highly effective precursor for ZnO synthesis, producing particles with small crystallite sizes, high crystallinity, and smooth surface morphology. This results in thin films with high optical transparency (80–95%), enhanced photocatalytic activity, and biocompatibility, making it ideal for optoelectronic applications. ZN also forms ZnO films with good (Nadia et al., 2020; Gatou et al., 2023a), but they typically have a rough, porous surface, which can improve surface reactivity (Nadia et al., 2020). However, its photocatalytic and bioactivity performance is generally lower than that of ZA, making it suitable for applications where surface texture is more important (Gatou et al., 2023a). In

https://doi.org/10.24191/mjcet.v8i2.8252

conclusion, ZA is preferred for high-performance films requiring superior photocatalytic efficiency and optical transparency, while ZN is better for applications needing moderate photocatalytic performance and surface roughness.

While extensive research has been conducted on optimizing synthesis parameters, the drying process has often been overlooked. Drying conditions, such as temperature, duration, and method, directly impact the morphology, structure, and functionality of the particles. Moderate temperatures like 60 °C allow controlled solvent evaporation, preserving porosity for applications like biosensing (Zhou et al., 2013). Higher temperatures like 100–120 °C remove moisture completely but may cause aggregation or alter morphology, which may reduce their effectiveness (Saputra et al., 2024). The drying time also affects the final properties of ZnO. Short durations, like 2 hours at 80 °C, yield semi-spherical particles (Rajeshkumar et al., 2023; Suciyati et al., 2024a; Suciyati et al., 2024b), while longer periods, such as 12 hours at 120 °C, enhance photocatalytic efficiency but risk clumping or structural damage (Saputra et al., 2024). Drying methods further refine properties. Oven drying is simple and produces uniform particles with antioxidant properties (Rajeshkumar et al., 2018), while vacuum drying minimises oxidation and aggregation (Yadav et al., 2024). Combining drying with calcination (e.g., 100 °C drying and 400 °C calcination) improves crystallinity and antibacterial properties (Endah et al., 2023).

These parameters must be finely tuned to optimise the drying process, addressing its often overlooked but essential role in ZnO synthesis. Therefore, this research will explore how drying temperature of 60, 70, and 80 °C affect the synthesis of ZnO from mango seed extract, while also examining how different zinc precursors, such as ZA and ZN, influence the synthesis process. By evaluating different drying temperature and precursor types, the study aims to understand their impact on the yield, size, and properties of the particles. The goal is to optimise these factors to improve the quality of the synthesised ZnO and provide new insights into how drying temperature and precursor choices affect particle synthesis.

2. MATERIAL AND METHOD

2.1 Materials and chemicals

The materials used in this study were Mango Gold Susu AA Grade seeds obtained from local beverages store in Selangor, Malaysia. Only seeds from mature mangoes were used as the main raw material for extract preparation to ensure a level of uniformity. Sigma-Aldrich® zinc acetate dihydrate ($Zn(CH_3COO)_2 \cdot 2H_2O$) and zinc nitrate hexahydrate ($Zn(NO_3)_2 \cdot 6H_2O$) were used as zinc precursors. These zinc precursors are labelled as ZA (zinc acetate) and ZN (zinc nitrate) throughout the experiment. 0.1 M sodium hydroxide solution (NaOH) was used for pH adjustment (Suciyati et al., 2024b). Ethanol and distilled water were used as solvents in washing and extraction.

2.2 Mango seed extract (MSE) preparation

The inner seeds were removed from the outer shells and thoroughly washed. The seeds were washed three times with tap water, followed by three times rinses with distilled water, and a final rinse using a solution of 100 mL ethanol diluted in 400 mL distilled water (Bekele et al., 2021). Then, the washed seeds were weighed and cut into small pieces. These pieces were dried at 60 °C until a constant weight was achieved, with the weight being measured hourly (Joshi et al., 2021). The dried seeds were ground into a fine powder and sieved for uniformity. A total of one gram of the powdered mango seed was mixed with

https://doi.org/10.24191/mjcet.v8i2.8252

100 mL of distilled water and stirred using a magnetic stirrer at 70 °C for 1 hour (Rajeshkumar et al., 2023). The resulting solution was filtered using Whatman No. 1 filter paper to obtain a clear solution, which was preserved at 4 °C (Joshi et al., 2021). Fig. 1 shows the illustration of the experimental set-up for MSE preparation.

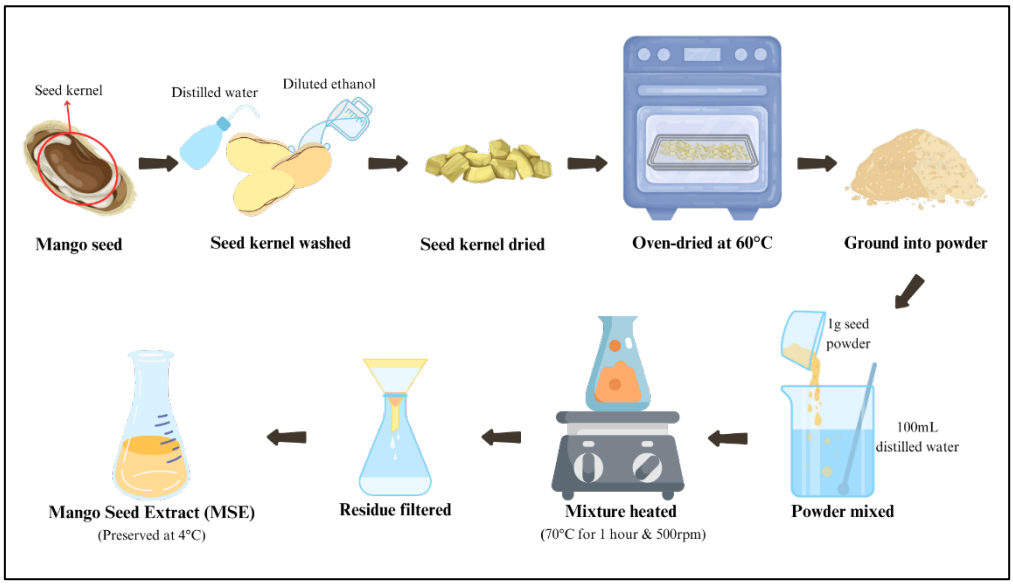

Fig. 1. Schematic illustration of MSE preparation

Source: Authors' own data

2.3 Zinc oxide particles synthesis

A 0.05 M of each zinc salt (Rajeshkumar et al., 2023) was prepared and mixed with 10 mL of mango seed extract (MSE) (Joshi et al., 2021). The pH of the mixture was adjusted to 8 using 0.1 M NaOH solution (Yadav et al., 2024). Then, the solutions were stirred with a magnetic stirrer at 70 °C for 1 hour (Bekele et al., 2021; Joshi et al., 2021; Suciyati et al., 2024b) at 500 rpm. The solution was then subjected to incubator shaker at 40 °C for one hour at 200 rpm. The mixture was then left at room temperature for one hour to separate the white precipitate from solution.

The resulting white precipitate was filtered and rinsed three times with distilled water (Li et al., 2020) and once with diluted ethanol (Endah et al., 2023; Suciyati et al., 2024a) to further remove the impurities. The precipitate was then dried at varying temperatures of 60 °C (Yadav et al., 2024; Zhou et al., 2013), 70 °C (Joshi et al., 2021), and 80 °C (Rajeshkumar et al., 2023; Suciyati et al., 2024a; Suciyati al., 2024b) until a constant weight was achieved, with the weight being measured hourly. The ZA samples were labelled as ZA60, ZA70, and ZA80, while the ZN samples were labelled as ZN60, ZN70, and ZN80. Finally, the dried precipitate was ground into a fine powder using a mortar (Rajeshkumar et al., 2023), and the final weight was recorded. Fig. 2 shows the illustration of the experimental set-up for ZnO particles synthesis.

https://doi.org/10.24191/mjcet.v8i2.8252

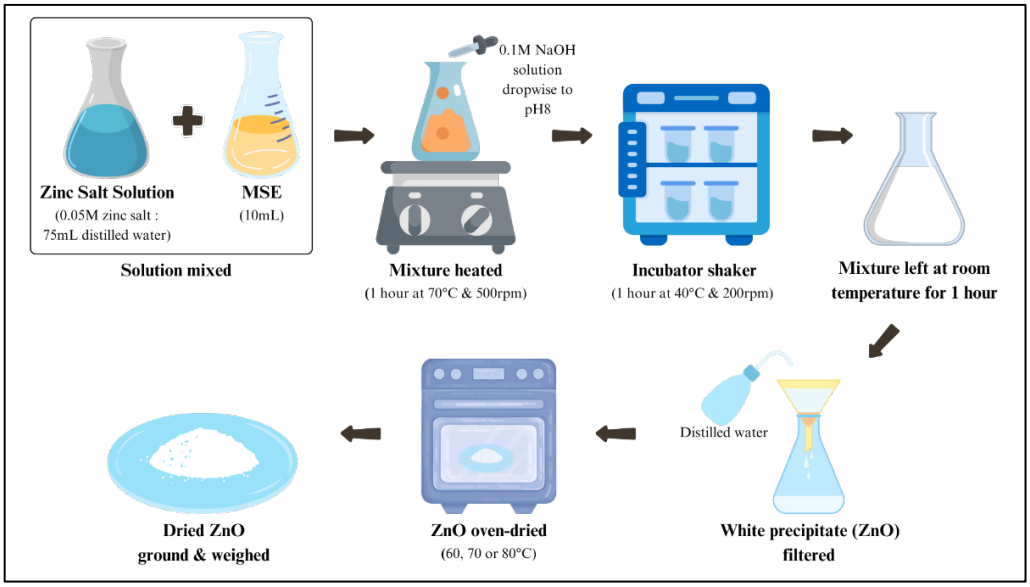

Fig. 2. Schematic illustration of ZnO synthesis from MSE

Source: Authors' own data

2.4 Characterisation techniques

Physical observation

The physical characteristics of the synthesised ZnO particles were first observed by examining the texture and colour of the dried powder.

Yield analysis

The initial weight of the zinc salt used and the final weight of the synthesised ZnO product obtained were recorded. To evaluate the efficiency of the synthesis, the extraction yield was calculated using the yield formula in Eq. (1) (Wang et al., 2022):

$$\text{Yield} = \frac{\text{Weight of ZnO Produced}}{\text{Weight of Zinc Salt}} \times 100\% \quad (1)$$

Scanning electron microscopy (SEM) and energy dispersive x-ray (EDX) spectroscopy

Scanning Electron Microscopy (SEM) is utilised to examine the surface morphology and particle size of the synthesised ZnO particles. Samples are kept in carbon-coated copper grid. The analysis is performed using a Hitachi SU3500 SEM, operating with a magnification range of 100× to 10,000× (Bekele et al., 2021).

Elemental analysis of the synthesised ZnO was performed using Energy dispersive x-ray (EDX) spectroscopy. The analysis was conducted at an accelerating voltage of 15 kV with a magnification of 27×, using the same machine as SEM (Ali et al., 2020). The detector takes off angle was set at 41.1°, and the live time was 30 seconds. The amplifier time was 3.84 μs, and the energy resolution was 126.1 eV. The

https://doi.org/10.24191/mjcet.v8i2.8252

EDX spectrum was used to confirm the elemental composition and purity of the synthesised ZnO particles (Ali et al., 2020).

Zeta potential and particle size

Zeta potential analysis was performed using a ZN3600 Zetasizer to determine the surface charge and colloidal stability of the synthesised ZnO. The measurement was conducted at a controlled temperature of 25 °C, using the dynamic light scattering (DLS) technique (Clogston & Patri, 2011). The refractive index (RI) of synthesised ZnO was set to 2.0, while the RI of the solvent system (acetic acid–water mixture) was estimated to be 1.333. Zeta potential values were interpreted based on standard stability criteria (Clogston & Patri, 2011). Particles with values greater than +30 mV or less than −30 mV were considered stable due to strong electrostatic repulsion, while values between−10 mV and +10 mV indicated low stability with a high tendency for agglomeration (Clogston & Patri, 2011).

The particle size of the synthesised ZnO was also measured using the same equipment via dynamic light scattering (DLS) at 25 °C. The same RI settings and absorption values as used in the zeta potential analysis were applied. The results were reported as the average hydrodynamic diameter and polydispersity index (PDI), which indicate the particle size distribution and degree of uniformity.

X-ray diffraction (XRD)

X-ray Diffraction (XRD) is employed to determine the crystalline structure, phase composition, and average crystallite size of the synthesised ZnO. The analysis is conducted using a Rigaku D/MAX-2000/PC diffractometer operating in continuous scan mode. The system is set to a voltage of 30 kV and a current of 40 mA (Suciyati et al., 2024a), utilising CuKα radiation with a wavelength of 1.5406 (Suciyati et al., 2024b). Data are collected over a 2θ range of 10° to 90° (Yadav et al., 2024), with a step size of 2°/min (Bekele et al., 2021).

The average crystallite size (D) of the synthesised ZnO was estimated using the Scherrer equation (Fatimah et al., 2021), as shown in Eq. (2):

$$D = \frac{K\lambda}{\beta \cos \theta} \tag{2}$$

where K is the Scherrer constant of 0.9, λ is the x-ray wavelength of 0.15406 nm, β is the full width at half maximum (FWHM) of the most intense diffraction peak (in radians), and θ is the Bragg angle (in radians).

Fourier-transform infrared spectroscopy (FTIR)

Fourier-transform infrared spectroscopy (FTIR) is used to characterise the functional groups associated with the synthesised ZnO. The analysis is performed using a PerkinElmer spectrometer, operating over a wavelength range of 4000 to 400 cm^{-1} with a resolution of 4 cm^{-1} (Abdullahi Ari et al., 2023).

Ultraviolet-visible (UV-vis) spectroscopy

Ultraviolet-visible (UV-Vis) spectroscopy is used to analyse the optical properties of the synthesised ZnO. The measurements are carried out using a PerkinElmer Lambda 750 spectrophotometer, covering a wavelength range of 250 to 800 nm because ZnO exhibits strong absorption in the UV and visible regions, typically between 200 to 400 nm (Suciyati, et al., 2024b; Yadav et al., 2024).

https://doi.org/10.24191/mjcet.v8i2.8252

The band gap energy of synthesised ZnO was calculated to gain deeper insight into its optical behaviour, a key factor influencing its overall effectiveness. The band gap energy was determined using Planck's equation (Junaid et al., 2023) , as shown in Eq. (3):

$$E = \frac{hc}{\lambda} \tag{3}$$

where E is the band gap energy (in eV), h is Planck's constant (4.14×10^{-15} eV·s), c is the speed of light (2.99×10^{8} m/s), and λ is the wavelength (in meters) taken from the UV-Vis spectrum.

3. RESULTS AND DISCUSSION

3.1 Physical observation

The drying temperature and type of zinc precursor influenced the physical appearance of synthesised ZnO as shown in Fig. 3. It shows that increasing the drying temperature from 60 to 80 °C made the synthesised ZnO powder appear finer and lighter in colour. For ZA samples, those dried at 60 °C were darker and had a coarse texture, while samples dried at 70 and 80 °C were lighter in colour and finer. This is because higher temperatures remove moisture more effectively, reducing clumping and producing a smoother powder. Study by (Shariffudin et al., 2012), shows a similar powder appearance for the drying temperatures of ZnO at elevated temperature from 100 to 300 °C.

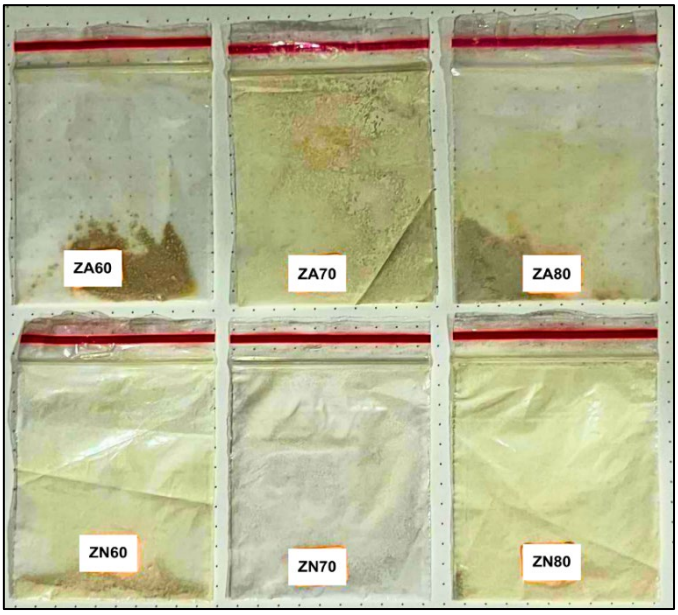

Fig. 3. ZnO appearance at various drying temperatures (ZA & ZN)

Source: Author's own data

https://doi.org/10.24191/mjcet.v8i2.8252

The type of zinc salt also affected the appearance and colour. ZA samples changed in texture and colour depending on the drying temperature. In contrast, ZN samples looked similar at all temperatures which are pale, cream-coloured, and very fine, like flour. This uniformity is due to ZN's better solubility and easier decomposition during synthesis, as also noted by (Riwayati et al., 2024).

3.2 Yield analysis

Table 1 demonstrates that higher drying temperatures led to more moisture loss, resulting in lower final weights and extraction yields. Free water evaporated at lower temperatures of 60 °C and below, contributing to the initial mass loss, whereas bound water was removed at higher temperatures of 70–80 °C, leading to structural changes in phytochemicals and reduced reduction efficiency, thereby lowering yield. Similar trends were seen for ZN samples, consistent with the explanation by (Donia et al., 2021) who explains that the decline in yield with increasing temperature is attributed to the removal of both free and bound water.

ZA gave higher yields than ZN at all drying temperatures. The highest yield of 37.80% was recorded for ZA60, while ZN60 gave only 20.54%, as ZN contains more water in its hexahydrate form, causing greater mass loss during drying (Kumar et al., 2018). In summary, ZA at 60 °C produced the highest extraction yield, while ZN gave finer texture but lower yield regardless of temperature.

Table 1. ZnO extraction yield (ZA & ZN)

Temperature, °C	Final weight, g		Extraction Yield, %	
	ZA	ZN	ZA	ZN
60	0.31	0.23	37.80	20.54
70	0.24	0.22	29.27	19.64
80	0.24	0.18	29.27	16.07

Source: Author's own data

3.3 Morphology and elemental analysis

SEM analysis showed that drying temperature affected the shape and agglomeration of the synthesised ZnO. As shown in Fig. 4, ZA samples dried at 60 °C produced large, agglomerated particles with rod-like shapes. At 70 °C, both rod and spherical particles appeared with less agglomeration, while at 80 °C, the particles became mostly spherical and more densely packed. Higher temperatures helped the particles grow in a more ordered way by improving crystallinity and promoting directional crystal growth. However, when the temperature increased further, the higher thermal energy caused the particles to move and collide more often, leading to stronger agglomeration. This balance between better shape and higher agglomeration agrees with the findings of (Limón-rocha et al., 2022), who reported that zinc acetate tends to form rod-like ZnO when dried at higher temperatures around 100 °C.

For ZN samples, spherical particles were seen at 60 and 70 °C with only slight agglomeration. At 80 °C, a flower-like structure with sharp edges appeared, possibly due to faster crystal growth at higher temperature. Similar shapes, such as spherical, semi-spherical, flake-like, and rice-like, have also been reported at drying temperatures between 80 and 100 °C (Bekele et al., 2021; Joshi et al., 2021; Rajeshkumar et al., 2018; Suciyati et al., 2024b).

https://doi.org/10.24191/mjcet.v8i2.8252

Overall, ZnO made from ZN showed more uniform and less agglomerated particles compared to ZA, especially at lower temperatures. A rod-like shape with controlled agglomeration is considered the best morphology for applications that need high surface area and good photoreactivity, such as antimicrobial coatings, because it improves light absorption and the production of reactive oxygen species.

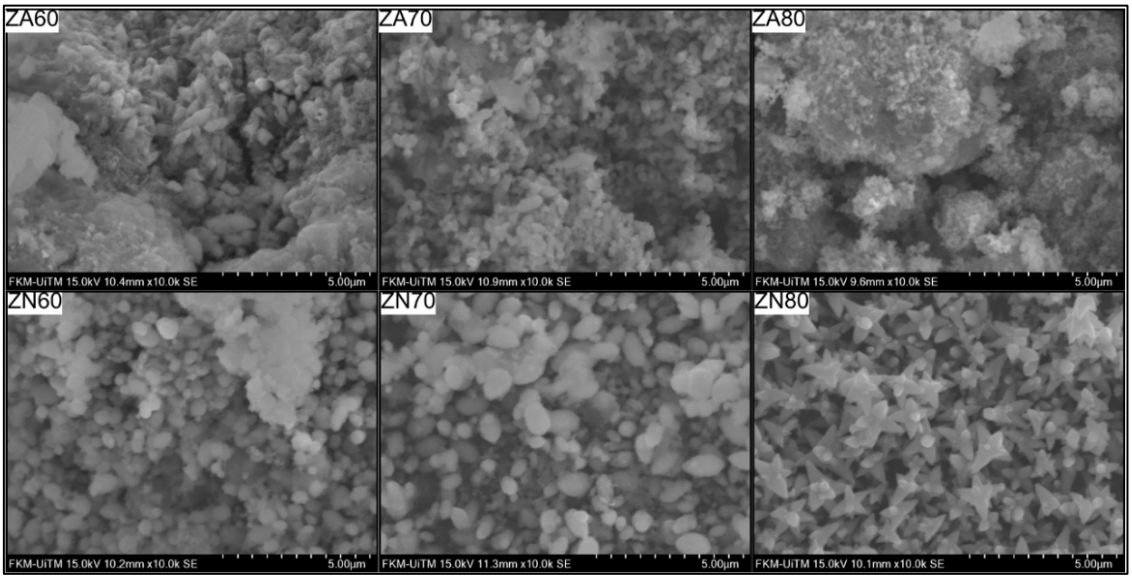

Fig. 4. SEM images of ZnO at 60 °C, 70 °C, 80 °C (ZA & ZN)

Source: Author's own data

EDX analysis confirmed that all synthesised ZnO contained only zinc (Zn) and oxygen (O) elements, as shown in Fig. 5. However, the composition was affected by both drying temperature and the type of precursor used. In theory, pure ZnO should have a 1:1 atomic ratio of Zn to O, which equals 50% Zn and 50% O atoms, as mentioned by (Skowronski et al., 2020) that the estimated Zn to O ratio is 1 to 1.6 with the increase of dying temperature from 100 to 200 °C (Skowronski et al., 2020). This value serves as the expected standard for comparison.

For ZA samples, drying at 60 and 70 °C resulted in Zn atomic percentages of 56.80% and 57.72%, respectively, both higher than the ideal 50%. Correspondingly, oxygen (O) content was slightly lower at around 43 to 44%, giving Zn to O ratios of approximately 1.32. These values suggest that drying at these temperatures may have favoured Zn-rich surfaces or partial oxidation (Skowronski et al., 2020). However, at 80 °C, a sharp increase in O atomic content to 73.90% and a decrease in Zn to 26.10% was observed, resulting in a Zn:O ratio of about 1:2.83. This significant deviation is due to surface oxidation or incomplete conversion at higher temperatures.

In contrast, ZN samples showed more stable and balanced Zn and O atomic ratios across all drying temperatures. Zn atomic content ranged from 50.25% to 51.79%, closely matching the theoretical 50% value, while O remained near 48 to 49%, giving Zn to O ratios around 1.05 to 1.08. This indicates that ZN provides a more consistent and complete reaction regardless of drying temperature. The improved

https://doi.org/10.24191/mjcet.v8i2.8252

performance of ZN is due to the better solubility and reactivity of ZN compared to ZA (Riwayati et al., 2024), especially during synthesis and drying. Higher solubility of ZN ensures more uniform precursor dispersion, leading to homogeneous nucleation and better-controlled particle size, which is advantageous for reproducible film incorporation and consistent optical properties.

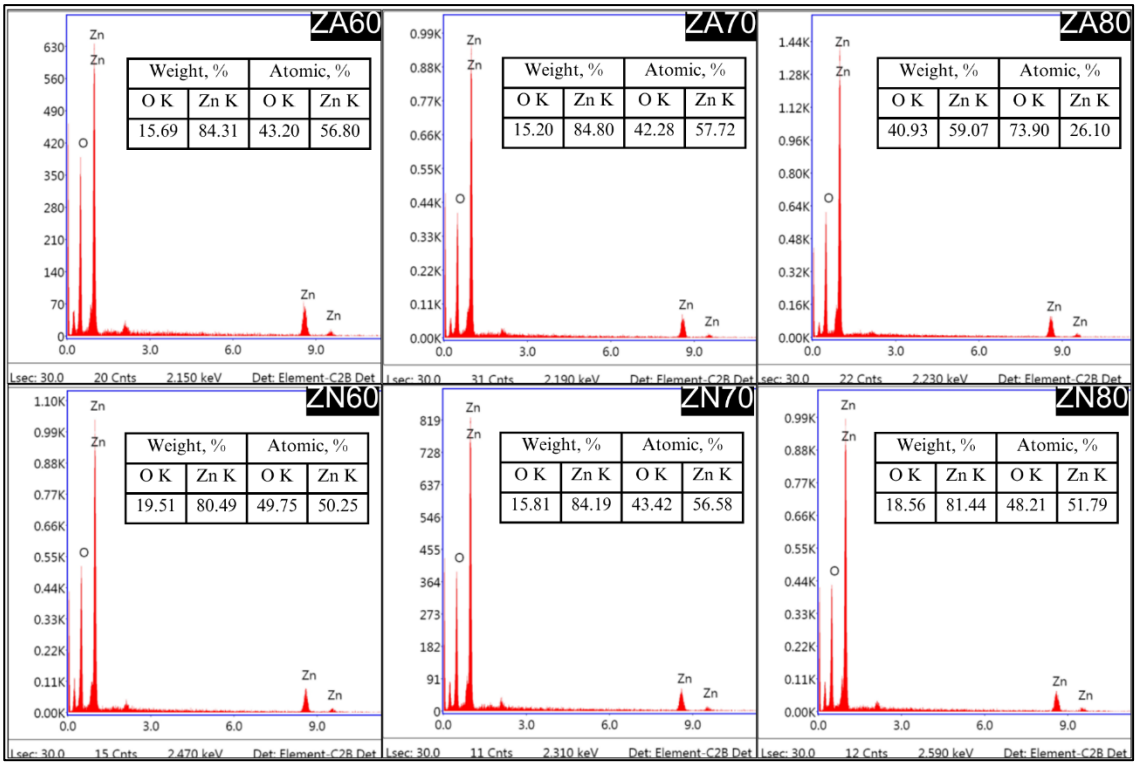

Fig. 5. EDX profiles of ZnO at 60 °C, 70 °C, 80 °C (ZA & ZN)

Source: Author's own data

3.4 Particle size and stability

Zeta potential analysis was used to measure the surface charge and stability of the synthesised ZnO. Based on Table 2, the drying temperature significantly affected the yield and color characteristics of ZA samples, indicating that higher temperatures reduced the amount of retained phytochemicals and influenced the formation of ZnO particles. At 60 and 70 °C, the zeta potential values were low and negative, −15.90 mV and −6.55 mV, respectively, showing weak stability. This helps explain the strong agglomeration seen in SEM at Section 3.2. At 80 °C, the zeta potential increased to a high positive value of +35.07 mV, indicating enhanced particle stability due to stronger electrostatic repulsion between particles. According to (Marsalek, 2014) and (Tran et al., 2024), zeta potential values exceeding ±30 mV generally reflect good colloidal stability. Despite this, some agglomeration was still observed in ZA80, likely due to particle growth at elevated temperatures. (Basri et al., 2020) similarly reported that heating during ZnO synthesis promotes agglomeration and results in larger particle sizes.

https://doi.org/10.24191/mjcet.v8i2.8252

Typically, ZnO particles carry a negative surface charge, so the positive value observed in ZA80 may be attributed to surface modifications by plant-derived compounds during drying. This is supported by (Vera et al., 2023) and (Alprol et al., 2024), who noted that organic constituents from plant extracts can influence the surface charge of synthesised ZnO particles. For ZN samples, the zeta potential remained negative and relatively stable across all drying temperatures, ranging from −22.03 to −24.60 mV. Although these values fall below the ±30 mV threshold typically associated with strong colloidal stability, their consistency reflects a stable surface charge and corresponds with the minimal agglomeration observed.

Table 2. Zeta potential of ZnO (ZA & ZN)

Temperature, °C	ZA		ZN	
	Zeta Potential, mV	**Standard Deviation (SD)**	**Zeta Potential, mV**	**Standard Deviation (SD)**
60	−15.90	±0.40	−22.03	±0.49
70	−6.55	±0.97	−22.87	±0.45
80	+35.07	±0.84	−24.60	±1.28

Source: Author's own data

Drying temperature also had a notable effect on the particle size of synthesised ZnO. For ZA samples, particle size increased from 1.487 µm at 60 °C to 2.338 µm at 70 °C, then slightly decreased to 2.082 µm at 80 °C. This trend suggests that moderate temperatures promoted particle growth, while higher temperatures may have restricted it due to rapid moisture loss. A similar pattern was observed by (Shariffudin et al., 2012), who reported an increase in ZnO grain size with drying temperatures up to 200 °C, followed by a decrease beyond that point, indicating a comparable growth–reduction behaviour despite different temperature ranges. In contrast, ZN samples showed a decrease in size from 2.325 µm at 60 °C to 1.454 µm at 70 °C, followed by a slight increase to 1.727 µm at 80 °C. Overall, ZN produced smaller and more uniform particles across the temperature range. This trend is supported by (Basri et al., 2020) and (Gatou et al., 2023b), who observed that temperature optimisation during chemical precipitation promotes the formation of smaller and more uniform ZnO particles. Fig. 6 demonstrates this temperature-dependent change in particle size.

In conclusion, ZA samples were more affected by changes in drying temperature, leading to unstable surface charge and larger particle sizes. Although ZA80 showed a strong positive zeta potential, which suggests good stability, some agglomeration still occurred, and the overall results were not consistent across temperatures. On the other hand, ZN samples showed more stable behaviour, with consistent negative zeta potential and smaller, more uniform particles at all temperatures. This suggests that ZN is a better and more reliable precursor for producing stable, well-dispersed ZnO particles.

3.5 Crystallite size and structure

XRD was used to confirm the crystal structure of the synthesised ZnO particles. All samples showed diffraction peaks that matched the standard pattern for hexagonal wurtzite ZnO (JCPDS card no. 36-1451), with main peaks at around 31.5°, 34.2°, and 36.0°, which correspond to the (100), (002), and (101) crystal planes, also reported by (Zhao et al., 2006) and (Ramike et al., 2023). The results are shown in Fig. 7 and Table 3. For ZA samples, the crystallite size increased with temperature, reaching the largest size of

https://doi.org/10.24191/mjcet.v8i2.8252

35.74 nm at 80 °C. This is because higher temperatures allow the particles to grow more, contributing to improved crystalline quality and increased grain size (Shariffudin et al., 2012). These results agree with the SEM images from Section 3.2, where larger and more compact synthesised ZnO particles were seen at higher temperatures, especially at 80 °C.

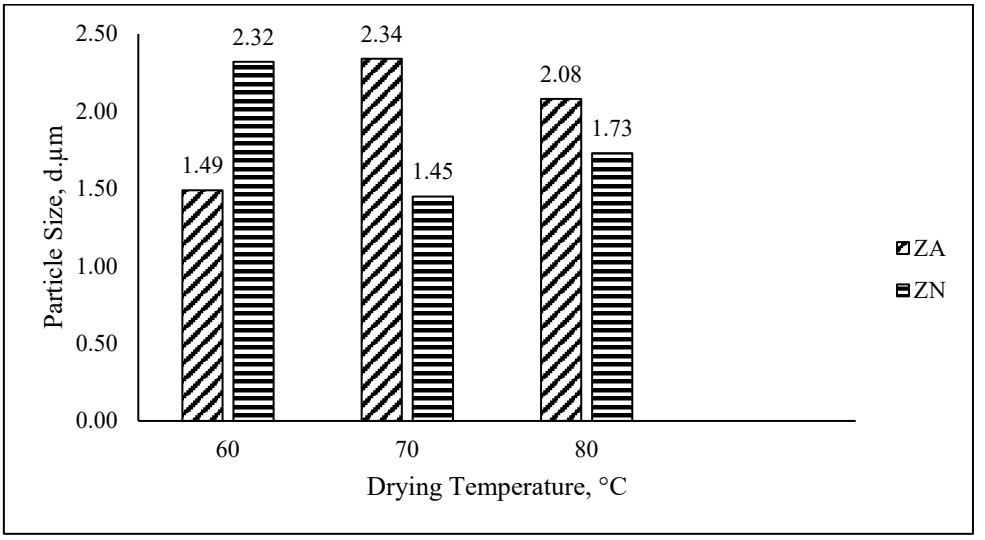

Fig. 6. Particle size of ZnO (ZA & ZN)

Source: Author's own data

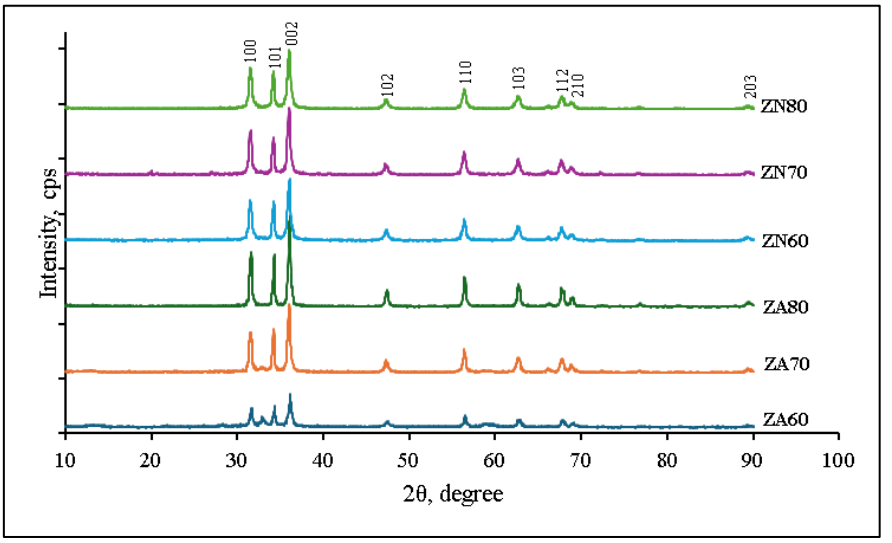

Fig.7. XRD of ZnO at 60 °C, 70 °C, 80 °C (ZA &ZN)

Source: Author's own data

https://doi.org/10.24191/mjcet.v8i2.8252

For ZN samples, the opposite trend was seen. Crystallite size slightly decreased as temperature increased, from 27.96 nm at 60 °C to 24.13 nm at 80 °C. This may be due to faster nucleation at high temperatures, which limits the growth of individual crystallites. (Zhao et al., 2006) observed that higher temperatures increase seed size and nucleation density, affecting ZnO morphology and growth. Data from SEM also support this, where the sample at 80 °C showed a flower-like shape with fine petals, a structure often linked with small crystallite size and fast formation (Ali et al., 2020; Bekele et al., 2021; Suciyati, et al., 2024b).

Table 3. Crystallite size of ZnO (ZA & ZN)

Temperature, °C	Crystallite size, nm	
	ZA	ZN
60	30.66	27.96
70	29.06	28.46
80	35.74	24.13

Source: Author's own data

Overall, both ZA and ZN produced ZnO with a wurtzite crystal structure, but ZN formed smaller and more uniform crystallites. The wurtzite phase is known for its excellent stability and high surface activity, which enhances photocatalytic efficiency, UV-blocking ability, and antimicrobial performance. Smaller crystallites also increase surface area and active sites, improving reactivity. These properties are particularly useful for intelligent packaging applications, where ZnO functions as an antimicrobial and UV-protective material to extend product shelf life.

3.6 Functional groups

FTIR analysis confirmed the formation of synthesised ZnO particles through the presence of Zn–O stretching vibrations in the 400–600 cm^{-1} range across all samples, consistent with reports by (Thongam et al., 2019) and (Handore et al., 2014). In addition, several expected functional groups were detected, as illustrated in Fig. 8. Broad peaks between 3278–3945 cm^{-1} were attributed to O–H and N–H bonds, likely originating from plant extracts and moisture, which aligns with the findings of (Ulker et al., 2025), who synthesised ZnO using *Tilia tomentosa*. Furthermore, peaks between 1384–2141 cm^{-1} indicated the presence of C=O or C=C groups, similar to observations by (Haji et al., 2025) using *Citrullus lanatus*. Additionally, peaks in the 900–1400 cm^{-1} region suggested C–H and C–O vibrations from organic residues, in agreement with (Hameed et al., 2023), who used green algae as a reducing agent.

Moreover, drying temperature significantly affects peak sharpness and intensity. At 80 °C, Zn–O peaks were clearer and organic-related peaks were reduced, suggesting better crystallinity and fewer residual compounds. This is further supported by (MuthuKathija et al., 2023), who reported less agglomeration of ZnO at 80 °C based on SEM analysis. In contrast, samples dried at 60 °C exhibited more organic-related peaks, likely due to incomplete drying. Additionally, precursor type influenced the FTIR results. ZA samples showed more organic-related peaks, especially above 1000 cm^{-1}, indicating the presence of remaining plant compounds. On the other hand, ZN samples exhibited cleaner spectra and stronger Zn–O signals, particularly at higher temperatures, suggesting better decomposition of organic matter and more complete synthesis (Riwayati et al., 2024).

https://doi.org/10.24191/mjcet.v8i2.8252

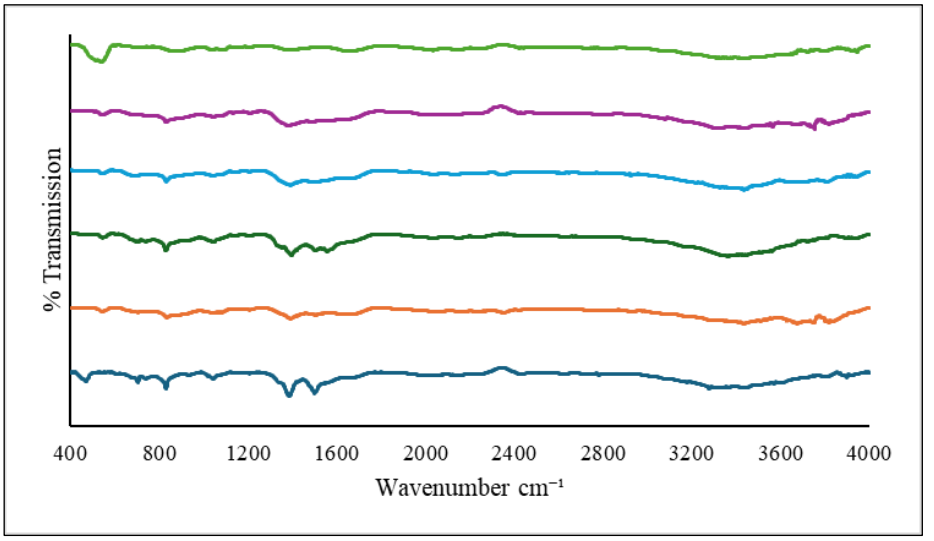

Fig. 8. FTIR of ZnO at 60 °C, 70 °C, 80 °C (ZA & ZN)

Source: Author's own data

Based on FTIR analysis, ZN is the better precursor for ZnO synthesis. It produced cleaner spectra with stronger Zn–O signals and fewer organic-related peaks, especially at higher drying temperatures, indicating more complete decomposition of plant compounds and better crystallinity. In contrast, ZA samples showed more residual organic peaks, suggesting less efficient removal of plant-based materials during drying. Therefore, ZN offers a more effective and controlled synthesis route for producing high-purity ZnO particles.

3.7 Optical properties

UV-Vis spectroscopy was employed to evaluate the optical properties of the synthesised ZnO, specifically by identifying absorption peaks and estimating band gap energy. This analysis reveals the material's ability to absorb ultra-violet (UV) light, which is essential for its effectiveness in UV-protective applications. According to (Arif et al., 2015), a higher band gap indicates stronger UV-blocking capability by enabling greater absorption of high-energy UV radiation. All ZnO samples showed absorption within the expected UV range of 200–400 nm, confirming successful synthesis. Notably, ZA samples displayed consistent absorption peaks between 269–273 nm, with the highest intensity of 4.08 A at 70 °C, suggesting that moderate drying enhances crystallinity and reduces agglomeration (Limón-rocha et al., 2022). ZN samples, on the other hand, showed strong absorption at 60 °C with absorption peak at 273 nm and intensity of 3.06 A. However, at 70 °C, the peak shifted to 334 nm with reduced intensity, and at 80 °C, no clear peak was observed, indicating poorer crystallinity and potential particle aggregation at elevated temperatures.

Furthermore, based on Table 4, band gap energy calculated using Planck's equation ranged from 3.71 to 4.61 eV, slightly above the standard ZnO range of 3.2 to 3.4 eV, due to nanoscale effects or surface interactions (Junaid et al., 2023). Among the ZA samples, the band gap values remained stable between 4.53 and 4.61 eV, with the lowest value at 70 °C, aligning with the highest absorption intensity and suggesting improved optical quality at this temperature. In contrast, ZN samples showed greater sensitivity

https://doi.org/10.24191/mjcet.v8i2.8252

to drying temperature; while the band gap was relatively high (4.54 eV) at 60 °C, it dropped sharply to 3.71 eV at 70 °C, and no measurable value was obtained at 80 °C due to the absence of a distinct peak. This is likely because of the structural degradation and poor crystallinity caused by excessive thermal decomposition of bioactive compounds, leading to incomplete ZnO formation. These findings indicate that ZA offers better thermal stability and consistent optical performance, whereas ZN is more prone to performance loss at higher temperatures.

Table 4. Bandgap energy of ZnO (ZA & ZN)

Temperature, °C	Wavelength, nm		Intensity, A		Bandgap Energy, eV	
	ZA	ZN	ZA	ZN	ZA	ZN
60	269	273	2.20	3.06	4.61	4.54
70	273	334	4.08	2.31	4.53	3.71
80	270	-	2.58	-	4.58	-

Source: Author's own data

4. CONCLUSION

This study successfully synthesised ZnO using mango seed extract via a green method and met all research objectives. It investigated the effects of drying temperature and compared zinc acetate (ZA) and zinc nitrate (ZN) precursors to identify optimal conditions for high-quality ZnO production. ZA samples consistently gave higher extraction yields, with the highest is 37.80% at 60 °C, while ZN samples produced finer and lighter powders. SEM and EDX confirmed ZN samples formed more uniform particles with a stable Zn:O 1 to 1 ratio. Zeta potential and particle size analysis showed ZN samples at 70 °C had the best stability of −24.60 mV and smallest, most consistent microparticles. XRD analysis revealed that all samples had a wurtzite structure. ZN samples had smaller crystallites, while ZA sample's crystallite size increased with temperature. FTIR showed ZA samples retained more plant residues, while ZN samples especially at 70 °C produced purer ZnO with stronger Zn–O signals. UV-Vis analysis found ZA samples at 70 °C had the highest absorption of 4.08 A at 273 nm and a stable bandgap of 4.53 eV, indicating better UV-shielding properties. ZN sample's optical performance declined above 70 °C, with no measurable bandgap at 80 °C. In summary, ZA sample at 60 °C offers high yield, ZA sample at 70 °C is ideal for UV protection, and ZN sample at 70 °C provides the best balance of stability, purity, and fine particle morphology, making it suitable for advanced applications.

ACKNOWLEDGEMENT

Special thanks are extended to Universiti Teknologi MARA, Shah Alam, for providing the facilities and resources necessary to carry out this study. Gratitude is also expressed to all individuals who contributed, whether directly or indirectly, to the successful completion of this research.

https://doi.org/10.24191/mjcet.v8i2.8252

CONFLICT OF INTEREST STATEMENT

The authors declare that no conflicts of interest, financial, personal, or professional, have influenced the outcomes of this research. This study was conducted independently and remains free from any competing interests.

AUTHORS' CONTRIBUTIONS

Nurainul Kamalia Iskandar Hussein: Conceptualisation, methodology, formal analysis, investigation and writing-original draft; **Rabiatul Adawiyah Abdol Aziz**: Conceptualisation, methodology, formal analysis and writing-original draft; **Siti Fatma Abd Karim**: Conceptualisation, review-editing and validation; **Ummi Kalthum Ibrahim**: Conceptualisation, review-editing, validation and funding acquisition.

REFERENCES

Abdullahi Ari, H., Adewole, A. O., Ugya, A. Y., Asipita, O. H., Musa, M. A., & Feng, W. (2023). Biogenic fabrication and enhanced photocatalytic degradation of tetracycline by bio structured ZnO nanoparticles. *Environmental Technology (United Kingdom)*, *44*(9), 1351–1366. https://doi.org/10.1080/09593330.2021.2001049

Ahmed, S., Annu, Chaudhry, S. A., & Ikram, S. (2017). A review on biogenic synthesis of ZnO nanoparticles using plant extracts and microbes: A prospect towards green chemistry. *Journal of Photochemistry and Photobiology B: Biology, 166*, 272–284. https://doi.org/10.1016/j.jphotobiol.2016.12.011

Al-darwesh, M. Y., Ibrahim, S. S., & Mohammed, M. A. (2024). A review on plant extract mediated green synthesis of zinc oxide nanoparticles and their biomedical applications. *Results in Chemistry, 7*, *101368*. https://doi.org/10.1016/j.rechem.2024.101368

Ali, K., Dwivedi, S., Azam, A., Saquib, Q., Al-Said, M. S., Alkhedhairy, A. A., & Musarrat, J. (2016). Aloe vera extract functionalized zinc oxide nanoparticles as nanoantibiotics against multi-drug resistant clinical bacterial isolates. *Journal of Colloid and Interface Science*, *472*, 145–156. https://doi.org/10.1016/j.jcis.2016.03.021

Ali, S. G., Ansari, M. A., Alzohairy, M. A., Alomary, M. N., Jalal, M., Alyahya, S., Asiri, S. M. M., & Khan, H. M. (2020). Effect of biosynthesized ZnO nanoparticles on multi-drug resistant pseudomonas aeruginosa. *Antibiotics*, *9*(5), 260. https://doi.org/10.3390/ANTIBIOTICS9050260

Alprol, A. E., Eleryan, A., Abouelwafa, A., Gad, A. M., & Hamad, T. M. (2024). Green synthesis of zinc oxide nanoparticles using *Padina pavonica* extract for efficient photocatalytic removal of methylene blue. *Scientific Reports*, *14*(1), 1–23. https://doi.org/10.1038/S41598-024-80757-9

Arif, A., Belahssen, O., Gareh, S., & Benramache, S. (2015). The calculation of band gap energy in zinc oxide films. *Journal of Semiconductors*, *36*(1). https://doi.org/10.1088/1674-4926/36/1/013001

Basnet, P., Inakhunbi Chanu, T., Samanta, D., & Chatterjee, S. (2018). A review on bio-synthesized zinc oxide nanoparticles using plant extracts as reductants and stabilizing agents. *Journal of Photochemistry and Photobiology B: Biology*, *183*, 201–221. https://doi.org/10.1016/j.jphotobiol.2018.04.036

https://doi.org/10.24191/mjcet.v8i2.8252

Basri, H. H., Talib, R. A., Sukor, R., Othman, S. H., & Ariffin, H. (2020). Effect of synthesis temperature on the size of ZnO nanoparticles derived from pineapple peel extract and antibacterial activity of ZnO–starch nanocomposite films. *Nanomaterials*, *10*(6), 1061. https://doi.org/10.3390/NANO10061061

Bekele, B., Degefa, A., Tesgera, F., Jule, L. T., Shanmugam, R., Priyanka Dwarampudi, L., Nagaprasad, N., & Ramasamy, K. (2021). Green versus chemical precipitation methods of preparing zinc oxide nanoparticles and investigation of antimicrobial properties. *Journal of Nanomaterials*, *2021,* 9210817. https://doi.org/10.1155/2021/9210817

Bhuyan, T., Mishra, K., Khanuja, M., Prasad, R., & Varma, A. (2015). Biosynthesis of zinc oxide nanoparticles from *Azadirachta indica* for antibacterial and photocatalytic applications. *Materials Science in Semiconductor Processing*, *32*, 55–61. https://doi.org/10.1016/j.mssp.2014.12.053

Bishop, K. J. M., Wilmer, C. E., Soh, S., & Grzybowski, B. A. (2009). Nanoscale forces and their uses in self-assembly. *Small* 5(14), 1600–1630. https://doi.org/10.1002/smll.200900358

Clogston, J. D., & Patri, A. K. (2011). Zeta potential measurement. *Methods in Molecular Biology*, *697*, 63–70. https://doi.org/10.1007/978-1-60327-198-1_6

Donia, D. T., Bauer, E. M., Missori, M., Roselli, L., Cecchetti, D., Tagliatesta, P., Gontrani, L., & Carbone, M. (2021). Room temperature syntheses of ZnO and their structures. *Symmetry*, *13*(4), 733. https://doi.org/10.3390/SYM13040733/S1

Endah, E. S., Saraswaty, V., Ratnaningrum, D., Kosasih, W., Ardiansyah, A., Risdian, C., Nugroho, P., Aji, E. S., & Setiyanto, H. (2023). Phyto-assisted synthesis of zinc oxide nanoparticles using mango (*Mangifera indica*) fruit peel extract and their antibacterial activity. *IOP Conference Series: Earth and Environmental Science*, *1201*(1). https://doi.org/10.1088/1755-1315/1201/1/012081

Fatimah, S., Ragadhita, R., Fitria, D., Husaeni, A., Bayu, A., & Nandiyanto, D. (2021). How to calculate crystallite size from x-ray diffraction (XRD) using Scherrer method. *ASEAN Journal of Science and Engineering*, *2*(1), 65-76. https://doi.org/10.17509/ajse.v2i1.37647

Gatou, M. A., Lagopati, N., Vagena, I. A., Gazouli, M., & Pavlatou, E. A. (2023a). ZnO nanoparticles from different precursors and their photocatalytic potential for biomedical use. *Nanomaterials*, *13*(1). https://doi.org/10.3390/nano13010122

Gatou, M. A., Kontoliou, K., Volla, E., Karachalios, K., Raptopoulos, G., Paraskevopoulou, P., Lagopati, N., & Pavlatou, E. A. (2023b). Optimization of ZnO nanoparticles' synthesis via precipitation method applying Taguchi robust design. *Catalysts, 13*(10), 1367. https://doi.org/10.3390/CATAL13101367

Haji, B. S., Barzinjy, A. A., Abbas, A. O., Kaygili, O., & Mousa, M. S. (2025). Green synthesis of ZnO nanoparticles using *Citrullus lanatus* fruit extract and their potential for microwave absorption. *Nano-Structures & Nano-Objects*, *43*, 101502. https://doi.org/10.1016/j.nanoso.2025.101502

Hameed, H., Waheed, A., Sharif, M. S., Saleem, M., Afreen, A., Tariq, M., Kamal, A., Al-onazi, W. A., Al Farraj, D. A., Ahmad, S., & Mahmoud, R. M. (2023). Green synthesis of zinc oxide (ZnO) nanoparticles from green algae and their assessment in various biological applications. *Micromachines*, *14*(5). https://doi.org/10.3390/mi14050928

Handore, K., Bhavsar, S., Horne, A., Chhattise, P., Mohite, K., Ambekar, J., Pande, N., & Chabukswar, V. (2014). Novel green route of synthesis of ZnO nanoparticles by using natural biodegradable polymer and its application as a catalyst for oxidation of aldehydes. *Journal of Macromolecular Science, Part A: Pure and Applied Chemistry*, *51*(12), 941–947. https://doi.org/10.1080/10601325.2014.967078

https://doi.org/10.24191/mjcet.v8i2.8252

Irede, E. L., Awoyemi, R. F., Owolabi, B., Aworinde, O. R., Kajola, R. O., Hazeez, A., Raji, A. A., Ganiyu, L. O., Onukwuli, C. O., Onivefu, A. P., & Ifijen, I. H. (2024). Cutting-edge developments in zinc oxide nanoparticles: synthesis and applications for enhanced antimicrobial and UV protection in healthcare solutions. *RSC Advances*, *14*(29), 20992–21034. https://doi.org/10.1039/d4ra02452d

Joshi, N. C., Malik, S., & Gururani, P. (2021). Utilization of polypyrrole/ZnO nanocomposite in the adsorptive removal of Cu^{2+}, Pb^{2+} and Cd^{2+} ions from wastewater. *Letters in Applied NanoBioScience*, *10*(3), 2339–2351. https://doi.org/10.33263/LIANBS103.23392351

Junaid, M., Ghulam Hussain, S., Abbas, N., & khan, W. Q. (2023). Band gap analysis of zinc oxide for potential bio glucose sensor. *Results in Chemistry*, *5*. https://doi.org/10.1016/j.rechem.2023.100961

Kumar, N., Banerjee, D., & Chavez, R. (2018). Exploring additives for improving the reliability of zinc nitrate hexahydrate as a phase change material (PCM). *Journal of Energy Storage*, *20*, 153–162. https://doi.org/10.1016/J.EST.2018.09.005

Li, X. X., Dong, J. Y., Li, Y. H., Zhong, J., Yu, H., Yu, Q. Q., & Lei, M. (2020). Fabrication of Ag–ZnO@ carboxymethyl cellulose/K-carrageenan/graphene oxide/konjac glucomannan hydrogel for effective wound dressing in nursing care for diabetic foot ulcers. *Applied Nanoscience (Switzerland)*, *10*(3), 729–738. https://doi.org/10.1007/s13204-019-01194-z

Limón-rocha, I., Guzmán-gonzález, C. A., Anaya-esparza, L. M., Romero-toledo, R., Rico, J. L., González-vargas, O. A., & Pérez-larios, A. (2022). Effect of the precursor on the synthesis of ZnO and its photocatalytic activity. *Inorganics, 10*(2), 16. https://doi.org/10.3390/INORGANICS10020016

Malaiappan, S., P T, P., & Niveditha, S. (2024). Green synthesis and characterization of zinc oxide nanoparticles using *Catharanthus roseus* extract: A Novel Approach. *Cureus, 16(5)*. https://doi.org/10.7759/cureus.60407

Marsalek, R. (2014). Particle Size and Zeta Potential of ZnO. *APCBEE Procedia*, *9*, 13–17. https://doi.org/10.1016/J.APCBEE.2014.01.003

MuthuKathija, M., Sheik Muhideen Badhusha, M., & Rama, V. (2023). Green synthesis of zinc oxide nanoparticles using Pisonia Alba leaf extract and its antibacterial activity. *Applied Surface Science Advances*, *15*, 100400. https://doi.org/10.1016/J.APSADV.2023.100400

Nadia, L., Attaf, A., Aida, M. S., Attaf, N., Othmane, M., & Bouaichi, F. (2020). Effect of different Zinc precursors in structural and optical properties of ZnO thin film*s*. *arXiv, 2003,*08487. https://doi.org/10.48550/arXiv.2003.08487

Rajeshkumar, S., Kumar, S. V., Ramaiah, A., Agarwal, H., Lakshmi, T., & Roopan, S. M. (2018). Biosynthesis of zinc oxide nanoparticles using *Mangifera indica l*eaves and evaluation of their antioxidant and cytotoxic properties in lung cancer (A549) cells. *Enzyme and Microbial Technology*, *117*, 91–95. https://doi.org/10.1016/j.enzmictec.2018.06.009

Rajeshkumar, S., Parameswari, R. P., Sandhiya, D., Al-Ghanim, K. A., Nicoletti, M., & Govindarajan, M. (2023). Green synthesis, characterization and bioactivity of mangifera indica seed-wrapped Zinc Oxide nanoparticles. *Molecules*, *28*(6). https://doi.org/10.3390/molecules28062818

Ramike, M. P., Ndungu, P. G., & Mamo, M. A. (2023). Exploration of the different dimensions of Wurtzite ZnO structure nanomaterials as gas sensors at room temperature. *Nanomaterials*, *13*(20), 2810. https://doi.org/10.3390/NANO13202810/S1

https://doi.org/10.24191/mjcet.v8i2.8252

Riwayati, I., Winardi, S., Madhania, S., Shimada, M., & Kusdianto. (2024). Green synthesis of ZnO nanoparticles using *Cosmos caudatus*: Effects of calcination temperature and precursor type on photocatalytic and antimicrobial activities. *Results in Engineering*, *24*, 103594. https://doi.org/10.1016/J.RINENG.2024.103594

Saputra, I. S., Nurfani, E., Fahmi, A. G., Saputro, A. H., Apriandanu, D. O. B., Annas, D., & Yulizar, Y. (2024). Effect of secondary metabolites from several leaf extracts on the green synthesized-ZnO nanoparticles. *Vacuum*, *227,* 113434. https://doi.org/10.1016/j.vacuum.2024.113434

Shafey, A. M. El. (2020). Green synthesis of metal and metal oxide nanoparticles from plant leaf extracts and their applications: A review. *Green Processing and Synthesis*, *9(*1), 304–339. https://doi.org/10.1515/gps-2020-0031

Shariffudin, S. S., Mamat, M. H., Herman, S. H., & Rusop, M. (2012). Influence of drying temperature on the structural, optical, and electrical properties of layer-by-layer ZnO nanoparticles seeded catalyst. *Journal of Nanomaterials*, *2012*, 359103. https://doi.org/10.1155/2012/359103

Skowronski, L., Ciesielski, A., Olszewska, A., Szczesny, R., Naparty, M., Trzcinski, M., & Bukaluk, A. (2020). Microstructure and optical properties of E-beam evaporated zinc oxide films-effects of decomposition and surface desorption. *Materials*, *13*(16). https://doi.org/10.3390/MA13163510

Suciyati, S. W., Junaidi, J., Situmeang, R., & Manurung, P. (2024a). Nano-ZnO prepared by using chaya and mango leaves extract for photocatalyst of methylene blue. *Journal of Metals, Materials and Minerals*, *34*(1). https://doi.org/10.55713/JMMM.V34I1.1848

Suciyati, S. W., Manurung, P., Junaidi, J., & Situmeang, R. (2024b). Optical and crystal structure properties of ZnO nanoparticle synthesized through biosynthesis method for photocatalysis Application. *Indonesian Journal of Chemistry*, *24*(1), 125–140. https://doi.org/10.22146/ijc.84796

Thirumal, S., Senthilkumar, S. R., & Sivakumar, T. (2014). Green tea (*Camellia sinensis*) mediated synthesis of zinc oxide (ZnO) nanoparticles and studies on their antimicrobial activities. In *Article in International Journal of Pharmacy and Pharmaceutical Sciences*. https://www.researchgate.net/publication/279565190

Thongam, D. D., Gupta, J., & Sahu, N. K. (2019). Effect of induced defects on the properties of ZnO nanocrystals: surfactant role and spectroscopic analysis. *SN Applied Sciences*, *1*, 1030. https://doi.org/10.1007/S42452-019-1058-3

Torres-León, C., Rojas, R., Contreras-Esquivel, J. C., Serna-Cock, L., Belmares-Cerda, R. E., & Aguilar, C. N. (2016). Mango seed: Functional and nutritional properties. *Trends in Food Science and Technology*, *55*, 109–117. https://doi.org/10.1016/j.tifs.2016.06.009

Tran, X. T., Bien, T. T. L., Tran, T. Van, & Nguyen, T. T. T. (2024). Biosynthesis of ZnO nanoparticles using aqueous extracts of *Eclipta prostrata* and *Piper longum*: Characterization and assessment of their antioxidant, antibacterial, and photocatalytic properties. *Nanoscale Advances*, *6*(19), 4885–4899. https://doi.org/10.1039/D4NA00326H

Ulker, G., Penlik, Y., & Gorduk, S. (2025). Synthesis, characterization and investigation of photocatalytic activity of ZnO Nanoparticles from *Tilia Tomentosa* (silverly linden) plant by green synthesis method. *Journal of Molecular Structure*, *1344*, 142929. https://doi.org/10.1016/J.MOLSTRUC.2025.142929

https://doi.org/10.24191/mjcet.v8i2.8252

Vera, J., Herrera, W., Hermosilla, E., Díaz, M., Parada, J., Seabra, A. B., Tortella, G., Pesenti, H., Ciudad, G., & Rubilar, O. (2023). Antioxidant activity as an indicator of the efficiency of plant extract-mediated synthesis of zinc oxide nanoparticles. *Antioxidants*, *12*(4), 784. https://doi.org/10.3390/ANTIOX12040784

Wang, Q., Mei, S., Manivel, P., Ma, H., & Chen, X. (2022). Zinc oxide nanoparticles synthesized using coffee leaf extract assisted with ultrasound as nanocarriers for mangiferin. *Current Research in Food Science*, *5*, 868–877. https://doi.org/10.1016/j.crfs.2022.05.002

Yadav, P., Manori, S., Chamoli, P., & Kumar Shukla, R. (2024). Photocatalytic degradation of ternary dye mixture using RGO, γ-Fe2O3 and ZnO based binary and ternary nanocomposites. *Inorganic Chemistry Communications*, *167*, 112791.https://doi.org/10.1016/j.inoche.2024.112791

Yudaev, P., Mezhuev, Y., & Chistyakov, E. (2022). Nanoparticle-containing wound dressing: antimicrobial and healing effects. *Gels*, *8*(6), 329. https://doi.org/10.3390/gels8060329

Zhao, J., Jin, Z. G., Li, T., & Liu, X. X. (2006). Nucleation and growth of ZnO nanorods on the ZnO-coated seed surface by solution chemical method. *Journal of the European Ceramic Society*, *26*(13), 2769–2775. https://doi.org/10.1016/J.JEURCERAMSOC.2005.07.062

Zhou, Y., Wang, L., Ye, Z., Zhao, M., Cai, H., & Huang, J. (2013). Mango core inner shell membrane template-directed synthesis of porous ZnO films and their application for enzymatic glucose biosensor. *Applied Surface Science*, *285*(Part B), 344–349. https://doi.org/10.1016/j.apsusc.2013.08.058

https://doi.org/10.24191/mjcet.v8i2.8252